JACS
JOURNAL OF THE AMERICAN CHEMICAL SOCIETY
pubs.acs.org/JACS
Article

Correlating Halide Segregation with Photolysis in Mixed-Halide Perovskites via In situ Opto-gravimetric Analysis

Zhaojian Xu, Xinjue Zhong, Tuo Hu, Junnan Hu, Antoine Kahn, and Barry P. Rand*

Cite This: J. Am. Chem. Soc. 2024, 146, 33368−33377
Read Online
ACCESS | Metrics & More | Article Recommendations | Supporting Information

ABSTRACT: Halide oxidation plays a fundamental role in halide segregation and the degradation of halide perovskites, yet quantitative measurement of halide oxidation in solid-state perovskite samples remains challenging. Herein, we demonstrate that in situ opto-gravimetric measurements based on a quartz crystal microbalance can quantify the photolysis kinetics of solid-state perovskites. By investigating a series of mixed bromide/iodide perovskites with varying halide ratios, we demonstrate identical compositional thresholds ($x \sim 0.4$ in the $CsPb(Br_xI_{1-x})_3$ system) for iodide oxidation, light-induced halide segregation, and photolysis. Our findings reveal the correlation between these light-induced instabilities and unambiguously explain the photolysis mechanism of mixed-halide perovskites. We also show that photolysis renders the perovskite film more *n*-type without involving lead reduction. This study introduces a powerful methodology for quantitatively analyzing the mass loss kinetics of halide perovskites under both practical operational and accelerated aging conditions, offering deeper insights into the mechanisms of perovskite degradation.

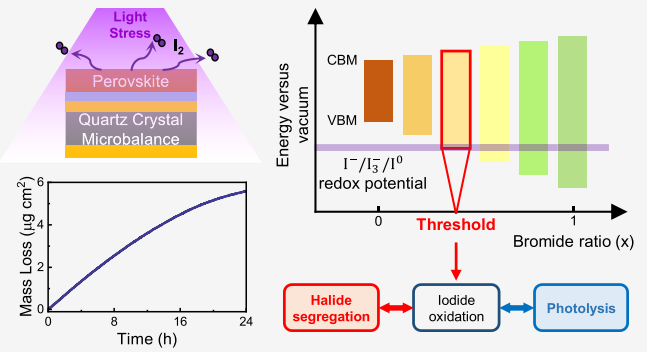

1. INTRODUCTION

As the efficiency of perovskite solar cells becomes competitive with that of silicon photovoltaics,[1] the intrinsic stability of halide perovskite materials under operational conditions, limited by various detrimental photoelectrochemical reactions[2,3] has become a primary focus. Halide oxidation, which plays an important role in initiating halide segregation,[4−7] halide vacancy densities,[4,8] and the degradation of halide perovskites,[8−11] is one of the most concerning photoelectrochemical reactions that may occur during perovskite device operation.[12,13] The prevailing method to study iodide oxidation and iodine expulsion kinetics involves immersing the perovskite film in an organic solvent and tracking the ultraviolet−visible (UV−vis) absorption spectra of the solvent under illumination, heat, or voltage bias.[8,14−21] However, the presence of solvent does not mimic the degradation of halide perovskite devices under practical solid-state conditions. More importantly, it has been reported that toluene, which is a prevailing choice as the solvent used in this type of measurement,[14,15,17,19−21] can be photo-oxidized in the presence of oxygen, catalyzed by perovskite nanoparticles.[22] The oxygen, either dissolved in the solvent or present in the environment, can also photo-oxidize iodide in various solvents.[23,24] These complicated interactions between perovskite and solvents under illumination hinder the accurate evaluation of halide oxidation using this approach. Thus, a direct and quantitative measurement of halide oxidation in solid-state perovskite samples under an inert environment is still required to investigate the kinetics of halide oxidation and understand its effects on perovskite photolysis.

The quartz crystal microbalance (QCM) was first introduced by Sauerbrey in 1959, who exploited the piezoelectric properties of quartz and derived a linear relationship between the frequency change of an oscillating quartz crystal and the deposited mass load.[25] Since then, owing to their exceptional sensitivity in mass measurements with the ability for in situ readout,[26] QCMs are employed in various applications, such as thin film deposition,[27,28] analytical electrochemistry,[29] and biosensing.[30,31] Previous studies have also demonstrated that QCMs are capable of determining the kinetics of photocatalytic decomposition on TiO_2 surfaces[32,33] and the photodegradation rate of organic compounds.[34−36] However, the possibility of using QCMs to investigate the degradation and mass loss kinetics of halide perovskite materials remains unexplored.

In this study, we show that a QCM can perform in situ opto-gravimetric analysis (OGA) of solid-state perovskite films to reveal the kinetics of iodide oxidation and photolysis of mixed-

Received: July 2, 2024
Revised: November 14, 2024
Accepted: November 15, 2024
Published: November 25, 2024

https://doi.org/10.1021/jacs.4c08939
J. Am. Chem. Soc. 2024, 146, 33368−33377

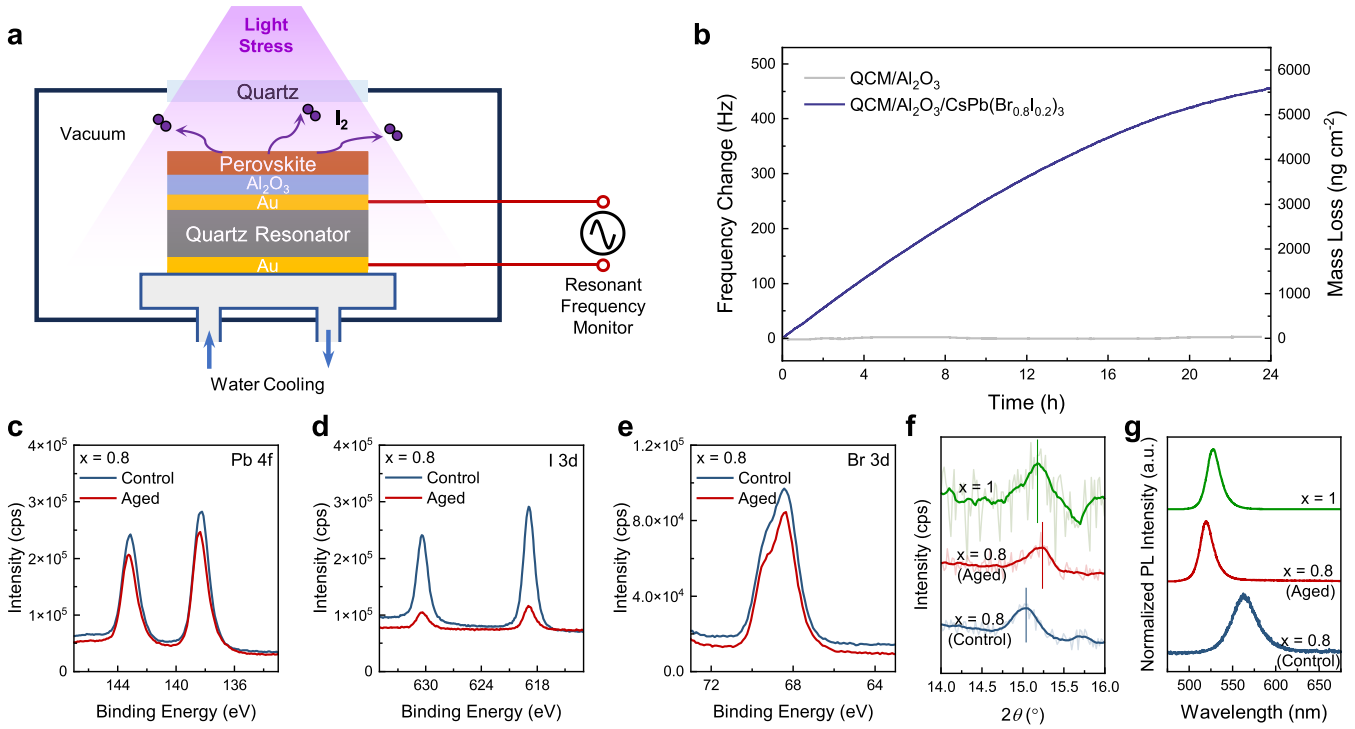

Figure 1. Photolysis of solid-state $CsPb(Br_{0.8}I_{0.2})_3$ thin films. (a) Schematic of the in situ OGA measurement. (b) In situ OGA measurements on blank QCM/Al_2O_3 and $QCM/Al_2O_3/CsPb(Br_{0.8}I_{0.2})_3$. (c–e) XPS measurements on $QCM/Al_2O_3/CsPb(Br_{0.8}I_{0.2})_3$ before (control) and after (aged) 75 mW cm^{-2} 370 nm UV aging under vacuum for 24 h: (c) Pb 4f, (d) I 3d, and (e) Br 3d spectra. (f) XRD measurements on $QCM/Al_2O_3/CsPb(Br_{0.8}I_{0.2})_3$ before (control) and after (aged) 75 mW cm^{-2} 370 nm UV aging under vacuum for 24 h, and a pristine $QCM/Al_2O_3/CsPbBr_3$ sample ($x = 1$) was also measured as a reference. (g) PL measurements on $QCM/Al_2O_3/CsPb(Br_{0.8}I_{0.2})_3$ before (control) and after (aged) 75 mW cm^{-2} 370 nm UV aging under vacuum for 24 h, and a pristine $QCM/Al_2O_3/CsPbBr_3$ sample ($x = 1$) was also measured as a reference.

halide perovskites. We start with a case study on $CsPb(Br_{0.8}I_{0.2})_3$ to demonstrate the preferential iodine loss with *n*-type self-doping under prolonged UV illumination. Furthermore, by varying the halide stoichiometry, we experimentally demonstrate the strong correlation between halide segregation and photolysis, revealing the key role of iodide oxidation in initiating both instabilities and determining the stability window. Finally, we study the effect of the A-site cation on the photolysis kinetics and highlight additional proton-induced mass loss pathways in halide perovskites with organic cations. These results introduce QCMs as a powerful tool for studying the photolysis kinetics of halide perovskite materials, highlighting their potential in advancing perovskite stability studies.

2. RESULTS AND DISCUSSION

2.1. Photolysis of Solid-State $CsPb(Br_{0.8}I_{0.2})_3$ Thin Films. Figure 1a shows the schematic of an in situ OGA measurement based on a QCM. In this experiment, we deposited perovskite films directly on QCM crystals, and by applying light stress and monitoring the change in resonant frequency of the QCM crystal, we can measure the mass loss from the perovskite during light aging in situ. To avoid potential ambiguities introduced by the catalytic effect of Au on perovskite photolysis[37] and/or charge injection from the electrode, we deposited a 20 nm Al_2O_3 layer on top of the QCM crystal by atomic layer deposition (ALD) to block direct contact between the perovskite and the Au electrode. Figure S1 shows the photos of samples at each step from a blank QCM crystal through Al_2O_3 and perovskite deposition. The Al_2O_3 coating does not change the morphology of the QCM surface, as evidenced by the scanning electron microscopy (SEM) images shown in Figure S2. Additionally, no Au signals were detected in the X-ray photoelectron spectroscopy (XPS) measurements after the Al_2O_3 coating (Figure S3), demonstrating the effective and conformal coverage of the Al_2O_3 buffer layer. The charge blocking effect of the Al_2O_3 buffer layer is further confirmed by the electrical measurements shown in Figure S4. An additional active water-cooling system was also attached to the QCM sensor to minimize the effects of heating on perovskite decomposition.

We start with Cs-based inorganic perovskites, which have been widely used in highly stable all-inorganic perovskite solar cells owing to their superior thermal stability,[38,39] to ensure that the halogen is the only volatile species in the film and that all the mass loss originates from halogen loss. All tested samples were aged under vacuum to minimize the readsorption of volatile degradation products, enabling accurate measurement of the mass loss. To begin with, we conducted in situ OGA measurements to measure the mass loss from $CsPb(Br_{0.8}I_{0.2})_3$ during UV aging as shown in Figure 1b, which is significantly distinct from the control measurement on a blank QCM/Al_2O_3 sample, demonstrating the effectiveness and sensitivity of the QCM in capturing perovskite mass loss. It should be noted that the temperature of the samples during the entire UV aging test was measured to be lower than 40 °C (Figure S5), thereby excluding the heating effect on perovskite mass loss and photolysis.[40]

To further reveal the mass loss and photolysis mechanism of $CsPb(Br_{0.8}I_{0.2})_3$, we did a series of characterizations on the $QCM/Al_2O_3/CsPb(Br_{0.8}I_{0.2})_3$ samples before and after UV aging for 24 h. Figure 1c–e shows the XPS results, where we use the Pb spectrum as a reference to calculate the relative

https://doi.org/10.1021/jacs.4c08939
J. Am. Chem. Soc. 2024, 146, 33368–33377

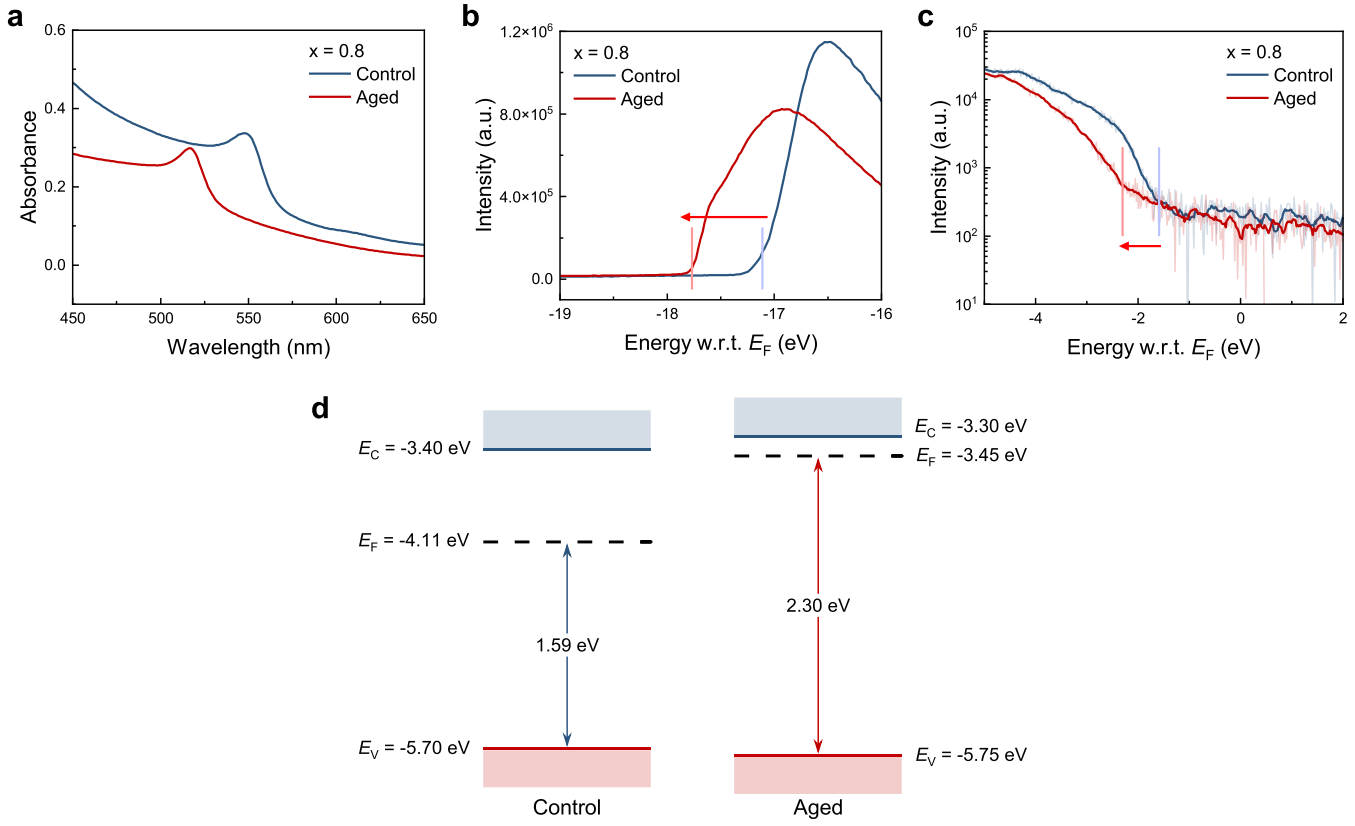

Figure 2. Effect of photolysis on electronic properties of $CsPb(Br_{0.8}I_{0.2})_3$ thin films. (a) UV−vis absorption measurements on ITO/$CsPb(Br_{0.8}I_{0.2})_3$ samples before (control) and after (aged) 75 mW cm^{-2} 370 nm UV aging under vacuum for 24 h. (b,c) UPS measurements on ITO/$CsPb(Br_{0.8}I_{0.2})_3$ samples before (control) and after (aged) 75 mW cm^{-2} 370 nm UV aging under vacuum for 24 h: (b) the secondary electron cutoff region and (c) the valence band maximum region. The aged sample was UV-illuminated again for 10 min in the UPS analysis chamber before data collection to enable UV reactivation. The rationale for this procedure is discussed in Note S1. (d) Energy level diagram of $CsPb(Br_{0.8}I_{0.2})_3$ thin films before (control) and after (aged) 75 mW cm^{-2} 370 nm UV aging under vacuum for 24 h.

concentration of iodine (I:Pb) and bromine (Br:Pb) before and after UV aging, shown in Table S1. We find that the I:Pb value decreases significantly after UV aging for 24 h, while the Br:Pb value shows negligible changes. These results indicate that the mass loss observed during in situ OGA measurements comes solely from iodine loss in mixed bromide/iodide perovskites. Furthermore, we also conducted X-ray diffraction (XRD) (Figure 1f) and photoluminescence (PL) (Figure 1g) measurements on the QCM/Al_2O_3/$CsPb(Br_{0.8}I_{0.2})_3$ samples before and after UV aging for 24 h. We find that the XRD peak of the aged sample shifts toward higher angles, accompanied by a PL blueshift. Both observations are consistent with the loss of iodine from the mixed-halide perovskites, causing the overall composition to become more bromide-rich, which has also been demonstrated in perovskite nanocrystals under prolonged illumination.[41−43] More surprisingly, the aged samples show an XRD peak at an even higher angle, together with higher-energy PL emissions, than those of the pure-bromide composition. These results are likely due to the formation of halide vacancies following iodine loss, which shrinks the lattice and leads to a higher bandgap.[5,44] Both XRD and PL measurements also indicate that the perovskite lattice structure is still maintained in the presence of a high concentration of halide vacancies following iodine loss, which is consistent with a previous report on the substantial defect tolerance of halide perovskites against halide vacancies.[45]

Iodine loss from Cs-based halide perovskites is most likely in the form of iodine vapor resulting from iodide oxidation. Since no Pb^0 signal (i.e., no Pb^{2+} reduction) was detected in XPS after UV aging (Figure 1c), the excess electrons will make the perovskite film more *n*-type following iodine loss. To study the effect of photolysis on the electronic properties of mixed-halide perovskites, we conducted UV−vis absorption and ultraviolet photoelectron spectroscopy (UPS) measurements on $CsPb(Br_{0.8}I_{0.2})_3$ samples before and after UV aging as shown in Figure 2. We find that the aged sample shows a blue-shifted absorption edge (Figure 2a), from which we extract the bandgap of $CsPb(Br_{0.8}I_{0.2})_3$ samples before and after UV aging using a fitting process that accounts simultaneously for the band edge and exciton contributions[46−48] (Figure S6). The UPS results demonstrate a smaller work function after UV aging (secondary electron cutoff, Figure 2b), accompanied by a Fermi level shift away from the valence band edge (Figure 2c). The resulting energy level diagrams of $CsPb(Br_{0.8}I_{0.2})_3$ samples before and after UV aging are shown in Figure 2d, which confirms a more *n*-type nature of the aged mixed-halide perovskite film. Additional discussion regarding the effect of UV excitation during UPS measurements[49,50] and the extra complexity caused by doping compensation[51] can be found in Note S1. This result is also consistent with a previous study that demonstrated spontaneous *n*-type self-doping of halide perovskites following iodine loss.[52] Combining the above experimental observations, we propose the following photolysis and mass loss chemical mechanism of $CsPb(Br_{0.8}I_{0.2})_3$ under UV irradiation:

https://doi.org/10.1021/jacs.4c08939
J. Am. Chem. Soc. 2024, 146, 33368−33377

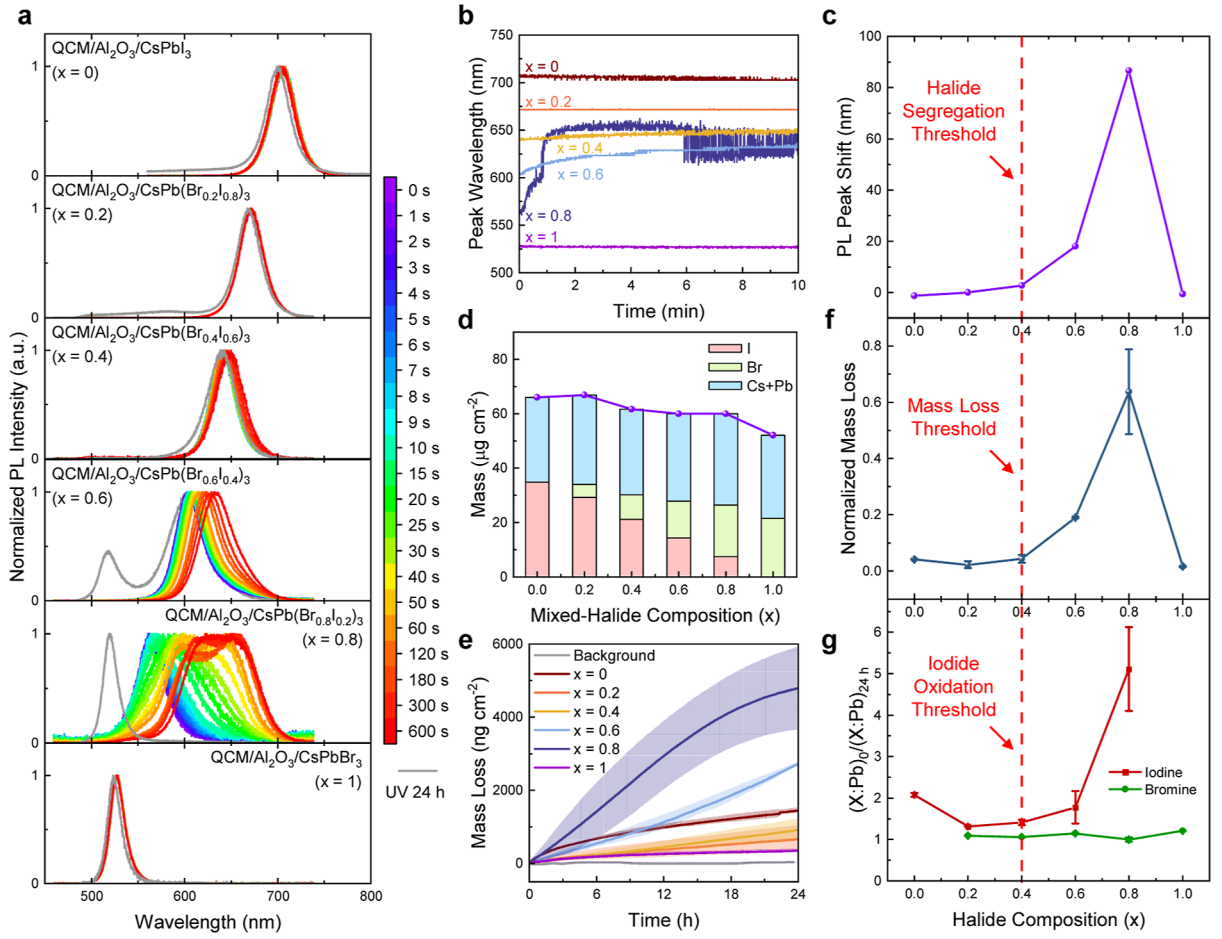

Figure 3. Correlation between halide segregation and photolysis in mixed-halide perovskites. (a) PL measurements on QCM/Al_2O_3/$CsPb(Br_xI_{1-x})_3$ (x between 0 and 1) during the initial 10 min continuous excitation (colored) and after 24 h UV aging (gray). All the PL measurements and UV aging were done in vacuum, and the excitation source for PL measurement (404 nm, 69 mW cm^{-2}) and the light source for UV aging (370 nm, 75 mW cm^{-2}) have the same photon flux to ensure consistency. (b) PL peak wavelength evolution of QCM/Al_2O_3/$CsPb(Br_xI_{1-x})_3$ samples during the initial 10 min continuous excitation. (c) PL peak shift of QCM/Al_2O_3/$CsPb(Br_xI_{1-x})_3$ samples after the initial 2 min continuous excitation. (d) Mass and stoichiometric component breakdown of $CsPb(Br_xI_{1-x})_3$ thin films measured by QCM. (e) In situ OGA measurements on QCM/Al_2O_3/$CsPb(Br_xI_{1-x})_3$, where the background data was measured on QCM/Al_2O_3. The shaded bands represent the standard deviation estimated from the measurements on two identical samples for each composition. (f) Normalized mass loss from QCM/Al_2O_3/$CsPb(Br_xI_{1-x})_3$ samples after 24 h UV aging. The mass loss is normalized by the mass of iodine for compositions with $0 \le x \le 0.8$, and by the mass of bromine for the pure-bromide composition ($x = 1$). The error bars represent the standard deviation estimated from the measurements on two identical samples for each composition. (g) Relative halide ratio change after 24 h UV aging. $(X:Pb)_0$ and $(X:Pb)_{24\,h}$ refer to the atomic ratio between halide and lead, estimated by XPS measurements, before and after 24 h UV aging, respectively. The error bars represent the standard deviation estimated from the XPS measurements on three different spots on the same sample.

$$10\ CsPb(Br_{0.8}I_{0.2})_3 \xrightarrow{\text{long-term UV, vacuum, room temperature}} 10\ CsPbBr_{2.4} + 3I_2 \uparrow + 6V^+_{halide} + 6e^- \quad (1)$$

2.2. Correlation between Halide Segregation and Photolysis in Mixed-Halide Perovskites. In addition to perovskite photolysis, halide segregation is another widely reported instability for mixed-halide perovskites that occurs under light illumination, which is often manifested as a PL redshift. In our previous study, we demonstrated the role of halide oxidation in halide segregation and indicated that iodide oxidation initiates halide segregation in mixed bromide/iodide perovskite.[4] As demonstrated in the previous section, the photolysis of mixed bromide/iodide perovskite and subsequent mass loss also result from iodide oxidation. Therefore, we hypothesize that halide segregation and photolysis in mixed-halide perovskite are correlated because they have the same origin, i.e., iodide oxidation. To demonstrate the correlation between halide segregation and photolysis, we tested a series of $CsPb(Br_xI_{1-x})_3$ compositions with x ranging from 0 to 1, and investigated the effect of mixed-halide stoichiometry on both halide segregation and photolysis.

We first measured the PL transients of various $CsPb(Br_xI_{1-x})_3$ samples during the initial 10 min of continuous excitation, as shown in Figure 3a. We find that both pure-halide perovskites ($x = 0$ and $x = 1$) and iodide-rich perovskites with $x < 0.4$ exhibit stable PL spectra, while the mixed-halide perovskites with $x > 0.4$ demonstrate a PL redshift over time, which can also be recovered after resting in the dark (Figure S11). Such a reversible PL redshift is widely interpreted as a sign of halide segregation, and the compositional threshold that we observed ($x = 0.4$) in $CsPb(Br_xI_{1-x})_3$ is also consistent with previous literature.[53] Since the rate of

https://doi.org/10.1021/jacs.4c08939
J. Am. Chem. Soc. 2024, 146, 33368−33377

halide segregation is directly reflected by the rate of PL redshift, we further extracted the PL peak wavelength as a function of time during the initial 10 min continuous excitation, as presented in Figure 3b. We observe that for the mixed-halide perovskites with $x > 0.4$, the rate of PL redshift becomes faster with a higher bromide ratio (x). Furthermore, the very bromide-rich composition ($x = 0.8$) began to show a slight PL blueshift toward the end of the 10 min PL transient test, which is a sign that iodine loss is starting to occur. Therefore, to exclude the effect of iodine loss in determining halide segregation kinetics, we used the PL peak shift within the first 2 min as an indicator to evaluate the rate of halide segregation for different halide compositions, as shown in Figure 3c. It also enables better visualization of the compositional threshold for halide segregation at $x = 0.4$.

Furthermore, to reflect the effect of photolysis, we also measured the PL spectra of those $CsPb(Br_xI_{1-x})_3$ samples after 24 h UV aging, as shown in Figure 3a. On the one hand, we find that a new emission peak, close to that of $CsPbBr_3$, appears in the PL spectra of mixed-halide perovskites with $x > 0.4$, which remains irreversible after resting in the dark (Figure S12). Such an observation indicates a significant amount of iodine loss and bromine enrichment in those mixed-halide perovskites after 24 h UV aging, as demonstrated in the case of $CsPb(Br_{0.8}I_{0.2})_3$ in Figure 1g. On the other hand, we observed only a small PL blueshift in both pure-halide perovskites ($x = 0$ and $x = 1$) and iodide-rich perovskites with $x < 0.4$ after 24 h UV aging, which is more likely due to defect formation, as demonstrated in our previous study, rather than changes in halide stoichiometry. More importantly, the concurrence of short-term PL redshift and long-term PL blueshift, with an identical compositional threshold at $x = 0.4$, emphasizes the underlying correlation between halide segregation and the photolysis of mixed-halide perovskites.

To quantitatively demonstrate the correlation between halide segregation and photolysis, we conducted additional in situ OGA measurements to reveal the kinetics of photolysis. We first measured the mass of each perovskite film by QCM and calculated the component breakdown based on each stoichiometry as shown in Figure 3d. Given that the fabrication process remains the same, a similar morphology is observed across different perovskite compositions, as shown in Figure S13. Furthermore, we conducted in situ OGA measurements on perovskites with different halide compositions during 24 h UV aging as shown in Figure 3e. The thickness of the perovskite layer deposited on the QCM substrate is much greater than the penetration depth of the 370 nm UV excitation used for in situ OGA measurements, ensuring complete absorption and the same dose of excitation across samples with different halide compositions for meaningful comparison. This is demonstrated in Figures S14−S16 and Table S2. We find that the mixed-halide perovskites with $x > 0.4$ show a significantly faster mass loss rate compared to other compositions. Nevertheless, all the samples showed negligible morphological changes after UV aging (Figure S13), indicating preserved structural integrity. As demonstrated in the case of $CsPb(Br_{0.8}I_{0.2})_3$, the mass loss observed during in situ OGA measurements comes solely from iodine loss in mixed bromide/iodide perovskites. To ensure a meaningful comparison, we normalized the mass loss by the mass of iodine for all iodide-containing compositions, and by the mass of bromine for the pure-bromide composition ($x = 1$). The normalized mass loss during and after 24 h UV aging is shown in Figures S17 and 3f, respectively, where we can identify a compositional threshold for mass loss at $x = 0.4$.

Additionally, to unambiguously identify the halogen species involved in mass loss during UV aging, we conducted XPS measurements on perovskite samples with different compositions to evaluate the stoichiometric changes after 24 h UV aging (Figure S18). The nonvolatile lead signal was used as a reference to calculate the relative content of different halogen species as summarized in Table S1. We used $(X{:}Pb)_0/(X{:}Pb)_{24\ h}$ as an indicator to reflect the stoichiometric changes after UV aging, where $(X{:}Pb)_0$ and $(X{:}Pb)_{24\ h}$ refer to the atomic ratio between halide and lead before and after 24 h UV aging, respectively. The $(X{:}Pb)_0/(X{:}Pb)_{24\ h}$ values for both bromide and iodide versus halide composition are displayed in Figure 3g. We find that the $(Br{:}Pb)_0/(Br{:}Pb)_{24\ h}$ value remains close to unity for all mixed-halide compositions, while all the $(I{:}Pb)_0/(I{:}Pb)_{24\ h}$ values are higher than unity. These results verify that the mass loss during UV aging comes solely from iodine loss in all iodine-containing compositions, while bromide remains in the film. More importantly, a similar threshold behavior for the iodine curve is observed in Figure 3g, indicating a similar compositional threshold for iodide oxidation at $x = 0.4$. It is worth noting that the pure-iodide perovskite ($CsPbI_3$) exhibits abnormal mass loss (Figure 3e) and iodine loss (Figure 3g), which is due to its unfavorable tolerance factor and intrinsic phase instability at room temperature.[54]

Combining Figure 3c,f,g, we observe a similar trend with an identical compositional threshold for halide segregation, mass loss, and iodide oxidation, which again highlights the correlation between halide segregation and photolysis. It should be noted that the samples for all the measurements shown in Figure 3 were fabricated on identical QCM/Al_2O_3 substrates to ensure consistency, thereby excluding any effect of different substrates on the results. To explain the correlation between halide segregation and photolysis, we propose the following scheme illustrated in Figure 4, which highlights the role of iodide oxidation in both halide segregation and photolysis, and explains the threshold behavior. In mixed bromide/iodide perovskites, the valence band maximum (VBM) becomes deeper with increased bromide ratio (x). On the one hand, for iodide-rich perovskites with a small x value, the energy of a hole, defined by the energy position of the VBM, is smaller than the oxidation potential of iodide. In this case, light-generated holes do not have sufficient oxidizing potential to oxidize iodide, making iodide oxidation unfavorable. On the other hand, when the bromide ratio increases and lowers the VBM sufficiently to make the energy of the hole larger than the oxidation potential of iodide, light-generated holes near the VBM can activate iodide oxidation. This explains the observed compositional threshold for iodide oxidation [$x = 0.4$ for $CsPb(Br_xI_{1-x})_3$], and the critical composition appears when the VBM crosses the iodide oxidation potential. Additionally, since the oxidation potential of bromide (light blue band) is larger than that of iodide (light purple band), iodide is oxidized first in mixed bromide/iodide perovskites, leading to preferential iodide oxidation and iodine loss during aging.

Based on the understanding of iodide oxidation, we can build a correlation between halide segregation and photolysis via iodide oxidation and explain the threshold behavior. Iodide oxidation upon illumination initially produces mobile oxidized iodide species. Under short-term illumination, when most

https://doi.org/10.1021/jacs.4c08939
J. Am. Chem. Soc. 2024, 146, 33368−33377

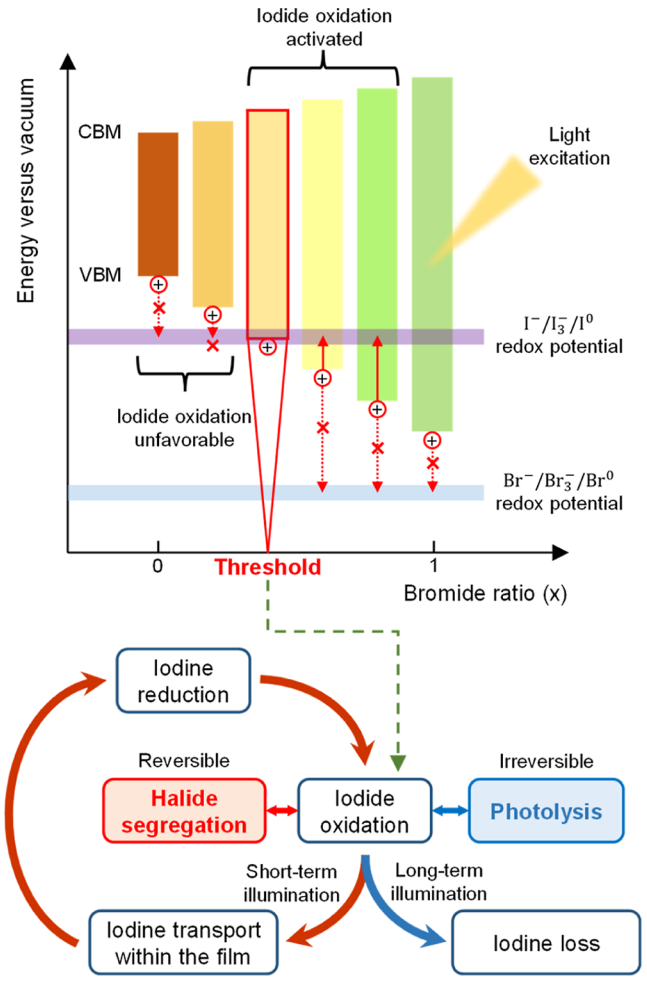

Figure 4. Schematic of the origin of iodide oxidation threshold and the correlation between iodide oxidation, halide segregation, and the photolysis of mixed bromide/iodide perovskites.

oxidized iodide species remain within the film, either as iodine interstitials or adsorbed to grain boundaries, these mobile species can move within the film, driven by spatial inhomogeneities. They may then be reduced and return to the lattice, forming an iodine transport circuit that relies exclusively on iodine redox chemistry without any need to invoke Pb redox. The preferential oxidation of iodide and the unbalanced transport fluxes of bromine and iodine lead to halide segregation, which is discussed in detail in our previous study.[4,6] On the other hand, under long-term illumination, the oxidized iodide species start to escape from the film and are irreversibly lost into the environment in the form of iodine vapor. Such irreversible iodine loss following iodide oxidation triggers the photolysis of the perovskite film.

In short, both halide segregation and photolysis are initiated by iodide oxidation, and therefore share the same compositional threshold. This explains the correlation between iodide oxidation, halide segregation, and the photolysis of mixed bromide/iodide perovskites. Furthermore, based on the experiments and discussions above, we can further generalize the photolysis mechanism for $CsPb(Br_{0.8}I_{0.2})_3$ to all Cs-based mixed bromide/iodide perovskites and explain their photolysis under UV irradiation:

$$CsPb(Br_xI_{1-x})_3 \xrightarrow{\text{long-term UV, vacuum, room temperature}} CsPbBr_{3x} + \frac{3(1-x)}{2}I_2 \uparrow + 3(1-x)V^+_{\text{halide}} + 3(1-x)e^- \quad (x > 0.4) \quad (2)$$

2.3. Effect of the A-Site Cation on Photolysis of Mixed-Halide Perovskites. Finally, we studied the effect of A-site cation composition on photolysis of mixed-halide perovskites. Compared to Cs-based perovskites where halogens are the only photolytic species accounting for mass loss, both methylammonium (MA)-based and formamidinium (FA)-based perovskites also possess volatilizable A-site cations. To investigate the effect of additional volatile species on mass loss, we first conducted in situ OGA measurements on $APb(Br_{0.8}I_{0.2})_3$ samples with different A-site cations as shown in Figure 5a, where the mass loss is normalized by the initial mass of each perovskite film. The component breakdown for each sample was calculated based on stoichiometry and shown in Figure S19. We find that both $FAPb(Br_{0.8}I_{0.2})_3$ and $MAPb(Br_{0.8}I_{0.2})_3$ exhibit significantly larger mass loss, with faster mass loss rates (the slope of the mass loss curve) at the beginning of UV aging compared to $CsPb(Br_{0.8}I_{0.2})_3$, demonstrating additional mass loss sourcing from the A-site cation. On the one hand, protons in MA^+ and FA^+ cations can accelerate halide oxidation and thus halogen loss by providing an additional reduction pair. On the other hand, proton transfer from MA^+ and FA^+ cations can also lead to the formation of HI and deprotonated amines, both of which are volatile and can directly contribute to mass loss.[55] These explain the observed trends of the in situ OGA measurements.

To confirm the species involved in the mass loss, we performed XPS measurements before and after UV aging as shown in Figures 5b,c and S20–S22. The absence of iodine signals (Figure 5b) and the presence of remaining bromine signals (Figures S20c, S21b, and S22b) in all three $APb(Br_{0.8}I_{0.2})_3$ samples after 100 h UV aging confirm the preferential and complete loss of iodine. In addition to iodine loss, both FA- and MA-based mixed-halide perovskites exhibit additional loss of A-site cations as indicated by the negligible nitrogen signals after UV aging (Figure 5c). Furthermore, we employed SEM measurements to study the effect of different A-site cations on morphological changes after UV aging, which are shown in Figure 5d–i. We observed that the Cs-based perovskite exhibited identical morphology before and after 100 h of UV aging, implying preserved perovskite structural integrity. This is also consistent with the observations from 24 h UV aging tests, as shown in Figure 1. These observations highlight the defect tolerance against halide vacancies in Cs-based perovskites, which is discussed in detail in Note S2. On the contrary, both FA- and MA-based perovskites showed significant morphological degradation after UV aging, resulting from concurrent mass loss of A-site cations and X-site anions, which destroys the perovskite structure. These observations demonstrate the additional mass loss pathway involved in the photolysis of FA- and MA-based halide perovskites and highlight the superior stability of Cs-based perovskites against photolysis compared to their hybrid organic–inorganic ammonium-based counterparts.

In addition, it should be noted that the method of using QCM for in situ OGA measurements is not limited to UV aging under vacuum, but also applicable for studying perovskite degradation kinetics under practical operational

https://doi.org/10.1021/jacs.4c08939
J. Am. Chem. Soc. 2024, 146, 33368–33377

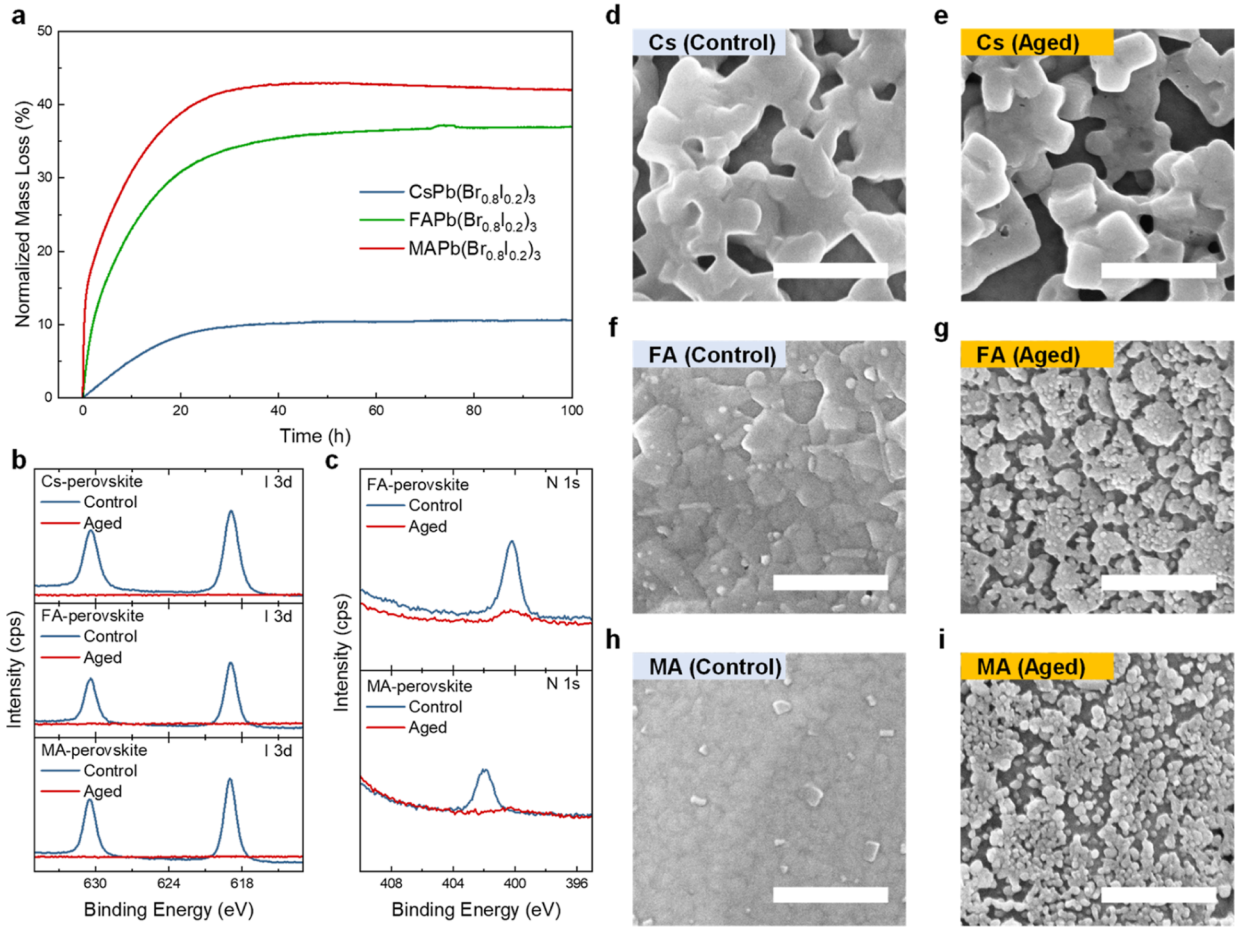

Figure 5. Effect of the A-site cation on photolysis of mixed-halide perovskites. (a) In situ OGA measurements on QCM/Al_2O_3/APb$(Br_{0.8}I_{0.2})_3$ with different A-site cations. The mass loss is normalized by the initial mass of each perovskite film. (b) I 3d XPS spectra of QCM/Al_2O_3/APb$(Br_{0.8}I_{0.2})_3$ with different A-site cations before (control) and after (aged) 75 mW cm^{-2} 370 nm UV aging under vacuum for 100 h. (c) N 1s XPS spectra of QCM/Al_2O_3/APb$(Br_{0.8}I_{0.2})_3$ with FA (top) and MA (bottom) cations before (control) and after (aged) 75 mW cm^{-2} 370 nm UV aging under vacuum for 100 h. (d–i) SEM images of QCM/Al_2O_3/APb$(Br_{0.8}I_{0.2})_3$ with different A-site cations before (control) and after (aged) 75 mW cm^{-2} 370 nm UV aging under vacuum for 100 h: (d,e) CsPb$(Br_{0.8}I_{0.2})_3$, (f,g) FAPb$(Br_{0.8}I_{0.2})_3$, and (h,i) MAPb$(Br_{0.8}I_{0.2})_3$. Scale bar, 500 nm.

conditions. To demonstrate this point, we further conducted in situ OGA measurements on a mixed-cation pure-iodide perovskite composition ($FA_{0.9}Cs_{0.1}PbI_3$ with 5% excess PbI_2, which is relevant for high-efficiency solar cell applications), under various aging conditions, including a practical condition for solar cell operation (atmospheric pressure and AM 1.5G illumination), as shown in Figure S23. Our method is able to capture mass loss in all cases, demonstrating its compatibility and effectiveness in studying perovskite degradation under practical operational conditions. Furthermore, no Pb^0 formation was observed in $FA_{0.9}Cs_{0.1}PbI_3$ samples, both with and without excess PbI_2, after UV aging (Figure S24). A detailed discussion on the absence of Pb^0 formation is provided in Note S3.

3. CONCLUSIONS

In summary, this work reveals the correlation between iodide oxidation, halide segregation, and photolysis of mixed-halide perovskites, and rationalizes the identical compositional threshold observed in these phenomena. These findings underscore the critical role of iodide oxidation in light-induced instabilities and elucidate the photolysis mechanism of mixed-halide perovskites. As iodide oxidation initiates both halide segregation and photolysis, it is important to develop effective strategies to mitigate iodide oxidation, which can help suppress these light-induced instabilities from the outset. We also show that iodide oxidation during photolysis is not necessarily accompanied by lead reduction; instead, the excess electrons make the perovskite film more *n*-type following iodine loss. Furthermore, we demonstrate the efficacy of using QCMs to study the photolysis process of halide perovskite materials, which provides a powerful tool to quantitatively evaluate the kinetics of perovskite degradation under both practical operational and accelerated aging conditions. This study not only advances our understanding of perovskite photolysis but also offers a facile and robust methodology for future research aimed at improving perovskite stability.

■ ASSOCIATED CONTENT

Supporting Information

The Supporting Information is available free of charge at https://pubs.acs.org/doi/10.1021/jacs.4c08939.

Experimental details (including materials used in this study, sample fabrication methods, and characterizations); photos of QCM substrates; SEM and XPS measurements on QCM substrates; electrical measurements demonstrating charge blocking by the Al_2O_3 buffer layer; temperature estimation; UV–vis absorption

https://doi.org/10.1021/jacs.4c08939
J. Am. Chem. Soc. 2024, 146, 33368–33377

measurements and corresponding Elliott fit; KP and UPS measurements and energy level diagram; PL recovery tests; SEM measurements on QCM/Al_2O_3/$CsPb(Br_xI_{1-x})_3$ samples with different halide stoichiometry; 370 nm UV light penetration depth estimation; XPS measurements on QCM/Al_2O_3/$CsPb(Br_xI_{1-x})_3$ samples with different halide stoichiometry; stoichiometric component breakdown and XPS measurements on QCM/Al_2O_3/$APb(Br_{0.8}I_{0.2})_3$ samples with different A-site cations; quantitative elemental analysis based on XPS measurements; in situ OGA measurements on QCM/Al_2O_3/$FA_{0.9}Cs_{0.1}PbI_3$ + 5% PbI_2 under different aging conditions and corresponding XPS measurements; comparison of perovskite film thickness and the penetration depth of 370 nm UV light; discussion on additional complexities caused by UV excitation during UPS measurements and dark recovery; discussion on defect tolerance against halide vacancies in Cs-based perovskites; discussion on the absence of Pb^0 formation under UV aging (PDF)

AUTHOR INFORMATION

Corresponding Author

Barry P. Rand − *Department of Electrical and Computer Engineering, Princeton University, Princeton, New Jersey 08544, United States; Andlinger Center for Energy and the Environment, Princeton University, Princeton, New Jersey 08544, United States;* orcid.org/0000-0003-4409-8751; Email: brand@princeton.edu

Authors

Zhaojian Xu − *Department of Electrical and Computer Engineering, Princeton University, Princeton, New Jersey 08544, United States;* orcid.org/0000-0003-2537-5354

Xinjue Zhong − *Department of Electrical and Computer Engineering, Princeton University, Princeton, New Jersey 08544, United States*

Tuo Hu − *Department of Electrical and Computer Engineering, Princeton University, Princeton, New Jersey 08544, United States*

Junnan Hu − *Department of Electrical and Computer Engineering, Princeton University, Princeton, New Jersey 08544, United States*

Antoine Kahn − *Department of Electrical and Computer Engineering, Princeton University, Princeton, New Jersey 08544, United States;* orcid.org/0000-0002-1612-3350

Complete contact information is available at: https://pubs.acs.org/10.1021/jacs.4c08939

Notes

The authors declare no competing financial interest.

ACKNOWLEDGMENTS

We acknowledge support for this work by the Department of the Navy, Office of Naval Research under ONR award no. N00014-23-1-2021. The authors acknowledge the use of the Imaging and Analysis Center (IAC) operated by the Princeton Materials Institute at Princeton University, which is supported in part by the Princeton Center for Complex Materials (PCCM), a National Science Foundation (NSF) Materials Research Science and Engineering Center (MRSEC; DMR-2011750). A.K. and X.Z. acknowledge supported by grant no. 2018349 from the United States-Israel Binational Science Foundation (BSF).

REFERENCES

(1) National Renewable Energy Laboratory, Best Research-Cell Efficiency Chart, https://www.nrel.gov/pv/cell-efficiency.html, accessed Nov. 20, 2024.

(2) Boyd, C. C.; Cheacharoen, R.; Leijtens, T.; McGehee, M. D. Understanding Degradation Mechanisms and Improving Stability of Perovskite Photovoltaics. *Chem. Rev.* **2019**, *119* (5), 3418−3451.

(3) Zhuang, J.; Wang, J.; Yan, F. Review on Chemical Stability of Lead Halide Perovskite Solar Cells. *Nano-Micro Lett.* **2023**, *15* (1), 84.

(4) Kerner, R. A.; Xu, Z.; Larson, B. W.; Rand, B. P. The Role of Halide Oxidation in Perovskite Halide Phase Separation. *Joule* **2021**, *5* (9), 2273−2295.

(5) Xu, Z.; Kerner, R. A.; Berry, J. J.; Rand, B. P. Iodine Electrochemistry Dictates Voltage-Induced Halide Segregation Thresholds in Mixed-Halide Perovskite Devices. *Adv. Funct. Mater.* **2022**, *32* (33), 2203432.

(6) Xu, Z.; Kerner, R. A.; Harvey, S. P.; Zhu, K.; Berry, J. J.; Rand, B. P. Halogen Redox Shuttle Explains Voltage-Induced Halide Redistribution in Mixed-Halide Perovskite Devices. *ACS Energy Lett.* **2023**, *8* (1), 513−520.

(7) Xu, Z.; Astridge, D. D.; Kerner, R. A.; Zhong, X.; Hu, J.; Hong, J.; Wisch, J. A.; Zhu, K.; Berry, J. J.; Kahn, A.; Sellinger, A.; Rand, B. P. Origins of Photoluminescence Instabilities at Halide Perovskite/Organic Hole Transport Layer Interfaces. *J. Am. Chem. Soc.* **2023**, *145* (21), 11846−11858.

(8) Motti, S. G.; Meggiolaro, D.; Barker, A. J.; Mosconi, E.; Perini, C. A. R.; Ball, J. M.; Gandini, M.; Kim, M.; De Angelis, F.; Petrozza, A. Controlling Competing Photochemical Reactions Stabilizes Perovskite Solar Cells. *Nat. Photonics* **2019**, *13* (8), 532−539.

(9) Hu, J.; Xu, Z.; Murrey, T. L.; Pelczer, I.; Kahn, A.; Schwartz, J.; Rand, B. P. Triiodide Attacks the Organic Cation in Hybrid Lead Halide Perovskites: Mechanism and Suppression. *Adv. Mater.* **2023**, *35* (40), 2303373.

(10) Akbulatov, A. F.; Luchkin, S. Y.; Frolova, L. A.; Dremova, N. N.; Gerasimov, K. L.; Zhidkov, I. S.; Anokhin, D. V.; Kurmaev, E. Z.; Stevenson, K. J.; Troshin, P. A. Probing the Intrinsic Thermal and Photochemical Stability of Hybrid and Inorganic Lead Halide Perovskites. *J. Phys. Chem. Lett.* **2017**, *8* (6), 1211−1218.

(11) Ren, X.; Wang, J.; Lin, Y.; Wang, Y.; Xie, H.; Huang, H.; Yang, B.; Yan, Y.; Gao, Y.; He, J.; Huang, J.; Yuan, Y. Mobile Iodides Capture for Highly Photolysis- and Reverse-Bias-Stable Perovskite Solar Cells. *Nat. Mater.* **2024**, *23* (6), 810−817.

(12) Zhu, H.; Teale, S.; Lintangpradipto, M. N.; Mahesh, S.; Chen, B.; McGehee, M. D.; Sargent, E. H.; Bakr, O. M. Long-Term Operating Stability in Perovskite Photovoltaics. *Nat. Rev. Mater.* **2023**, *8* (9), 569−586.

(13) Xu, Z.; Kerner, R. A.; Kronik, L.; Rand, B. P. Beyond Ion Migration in Metal Halide Perovskites: Toward a Broader Photoelectrochemistry Perspective. *ACS Energy Lett.* **2024**, *9*, 4645−4654.

(14) Kim, G. Y.; Senocrate, A.; Yang, T.-Y.; Gregori, G.; Grätzel, M.; Maier, J. Large Tunable Photoeffect on Ion Conduction in Halide Perovskites and Implications for Photodecomposition. *Nat. Mater.* **2018**, *17* (5), 445−449.

(15) Wang, S.; Jiang, Y.; Juarez-Perez, E. J.; Ono, L. K.; Qi, Y. Accelerated Degradation of Methylammonium Lead Iodide Perovskites Induced by Exposure to Iodine Vapour. *Nat. Energy* **2016**, *2* (1), 16195.

(16) Samu, G. F.; Balog, A.; De Angelis, F.; Meggiolaro, D.; Kamat, P. V.; Janáky, C. Electrochemical Hole Injection Selectively Expels Iodide from Mixed Halide Perovskite Films. *J. Am. Chem. Soc.* **2019**, *141* (27), 10812−10820.

(17) Lin, Y.-H.; Sakai, N.; Da, P.; Wu, J.; Sansom, H. C.; Ramadan, A. J.; Mahesh, S.; Liu, J.; Oliver, R. D. J.; Lim, J.; Aspitarte, L.; Sharma, K.; Madhu, P. K.; Morales-Vilches, A. B.; Nayak, P. K.; Bai, S.; Gao, F.; Grovenor, C. R. M.; Johnston, M. B.; Labram, J. G.; Durrant, J. R.; Ball, J. M.; Wenger, B.; Stannowski, B.; Snaith, H. J. A

Piperidinium Salt Stabilizes Efficient Metal-Halide Perovskite Solar Cells. *Science* **2020**, *369* (6499), 96−102.
(18) Mathew, P. S.; Samu, G. F.; Janáky, C.; Kamat, P. V. Iodine (I) Expulsion at Photoirradiated Mixed Halide Perovskite Interface. Should I Stay or Should I Go? *ACS Energy Lett.* **2020**, *5* (6), 1872−1880.
(19) Yang, X.; Ni, Y.; Zhang, Y.; Wang, Y.; Yang, W.; Luo, D.; Tu, Y.; Gong, Q.; Yu, H.; Zhu, R. Multiple-Defect Management for Efficient Perovskite Photovoltaics. *ACS Energy Lett.* **2021**, *6* (7), 2404−2412.
(20) Chen, S.; Xiao, X.; Gu, H.; Huang, J. Iodine Reduction for Reproducible and High-Performance Perovskite Solar Cells and Modules. *Sci. Adv.* **2021**, *7* (10), No. eabe8130.
(21) Zhou, Y.; van Laar, S. C. W.; Meggiolaro, D.; Gregori, L.; Martani, S.; Heng, J.-Y.; Datta, K.; Jiménez-López, J.; Wang, F.; Wong, E. L.; Poli, I.; Treglia, A.; Cortecchia, D.; Prato, M.; Kobera, L.; Gao, F.; Zhao, N.; Janssen, R. A. J.; De Angelis, F.; Petrozza, A. How Photogenerated I_2 Induces I-Rich Phase Formation in Lead Mixed Halide Perovskites. *Adv. Mater.* **2024**, *36* (1), 2305567.
(22) Huang, H.; Yuan, H.; Zhao, J.; Solís-Fernández, G.; Zhou, C.; Seo, J. W.; Hendrix, J.; Debroye, E.; Steele, J. A.; Hofkens, J.; Long, J.; Roeffaers, M. B. J. C(sp^3)−H Bond Activation by Perovskite Solar Photocatalyst Cell. *ACS Energy Lett.* **2019**, *4* (1), 203−208.
(23) Levanon, H.; Navon, G. Spectrum and Stability of Oxygen Iodide Charge-Transfer Complex. *J. Phys. Chem.* **1969**, *73* (6), 1861−1868.
(24) Rohatgi-Mukherjee, K. K.; Gupta, A. K. Anthracene Sulphonate Sensitized Photooxidation of Iodide Ion in Aqueous Solution Via Singlet Oxygen. *Chem. Phys. Lett.* **1977**, *46* (2), 368−371.
(25) Sauerbrey, G. Verwendung Von Schwingquarzen Zur Wägung Dünner Schichten Und Zur Mikrowägung. *Z. Physik* **1959**, *155* (2), 206−222.
(26) Wang, L.; Song, J.; Yu, C. The Utilization and Advancement of Quartz Crystal Microbalance (QCM): A Mini Review. *Microchem. J.* **2024**, *199*, 109967.
(27) Czanderna, A. W.; Lu, C. Introduction, History, and Overview of Applications of Piezoelectric Quartz Crystal Microbalances. *Methods and Phenomena*; Lu, C., Czanderna, A. W., Eds.; Elsevier, 1984; Vol. 7, pp 1−18.
(28) Wajid, A. On the Accuracy of the Quartz-Crystal Microbalance (QCM) in Thin-Film Depositions. *Sens. Actuators, A* **1997**, *63* (1), 41−46.
(29) Buttry, D. A.; Ward, M. D. Measurement of Interfacial Processes at Electrode Surfaces with the Electrochemical Quartz Crystal Microbalance. *Chem. Rev.* **1992**, *92* (6), 1355−1379.
(30) Marx, K. A. Quartz Crystal Microbalance: A Useful Tool for Studying Thin Polymer Films and Complex Biomolecular Systems at the Solution−Surface Interface. *Biomacromolecules* **2003**, *4* (5), 1099−1120.
(31) Alanazi, N.; Almutairi, M.; Alodhayb, A. N. A Review of Quartz Crystal Microbalance for Chemical and Biological Sensing Applications. *Sens. Imag.* **2023**, *24* (1), 10.
(32) Nakamura, Y.; Katou, Y.; Rengakuji, S. QCM Method to Evaluate Photocatalyst Ability of TiO_2. *Electrochemistry* **2004**, *72* (6), 408−411.
(33) Abe, T.; Kato, H. Real-Time Measurement of Photocatalytic Reactions Using a Monolithic QCM Array. *J. Micromech. Microeng.* **2009**, *19* (9), 094019.
(34) Malecha, K. T.; Cai, Z.; Nizkorodov, S. A. Photodegradation of Secondary Organic Aerosol Material Quantified with a Quartz Crystal Microbalance. *Environ. Sci. Technol. Lett.* **2018**, *5* (6), 366−371.
(35) Baboomian, V. J.; Gu, Y.; Nizkorodov, S. A. Photodegradation of Secondary Organic Aerosols by Long-Term Exposure to Solar Actinic Radiation. *ACS Earth Space Chem.* **2020**, *4* (7), 1078−1089.
(36) Alodhayb, A. N. Measurement of Polystyrene Photodegradation Rate Using a Quartz Crystal Microbalance. *IET Nanobiotechnol.* **2022**, *16* (2), 61−65.
(37) Kerner, R. A.; Schulz, P.; Christians, J. A.; Dunfield, S. P.; Dou, B.; Zhao, L.; Teeter, G.; Berry, J. J.; Rand, B. P. Reactions at Noble Metal Contacts with Methylammonium Lead Triiodide Perovskites: Role of Underpotential Deposition and Electrochemistry. *APL Mater.* **2019**, *7* (4), 041103.
(38) Liang, J.; Wang, C.; Wang, Y.; Xu, Z.; Lu, Z.; Ma, Y.; Zhu, H.; Hu, Y.; Xiao, C.; Yi, X.; Zhu, G.; Lv, H.; Ma, L.; Chen, T.; Tie, Z.; Jin, Z.; Liu, J. All-Inorganic Perovskite Solar Cells. *J. Am. Chem. Soc.* **2016**, *138* (49), 15829−15832.
(39) Zhao, X.; Liu, T.; Burlingame, Q. C.; Liu, T.; Holley, R.; Cheng, G.; Yao, N.; Gao, F.; Loo, Y.-L. Accelerated Aging of All-Inorganic, Interface-Stabilized Perovskite Solar Cells. *Science* **2022**, *377* (6603), 307−310.
(40) Akbulatov, A. F.; Ustinova, M. I.; Shilov, G. V.; Dremova, N. N.; Zhidkov, I. S.; Kurmaev, E. Z.; Frolova, L. A.; Shestakov, A. F.; Aldoshin, S. M.; Troshin, P. A. Temperature Dynamics of $MAPbI_3$ and PbI_2 Photolysis: Revealing the Interplay between Light and Heat, Two Enemies of Perovskite Photovoltaics. *J. Phys. Chem. Lett.* **2021**, *12* (18), 4362−4367.
(41) Zhang, H.; Fu, X.; Tang, Y.; Wang, H.; Zhang, C.; Yu, W. W.; Wang, X.; Zhang, Y.; Xiao, M. Phase Segregation Due to Ion Migration in All-Inorganic Mixed-Halide Perovskite Nanocrystals. *Nat. Commun.* **2019**, *10* (1), 1088.
(42) Brennan, M. C.; Toso, S.; Pavlovetc, I. M.; Zhukovskyi, M.; Marras, S.; Kuno, M.; Manna, L.; Baranov, D. Superlattices Are Greener on the Other Side: How Light Transforms Self-Assembled Mixed Halide Perovskite Nanocrystals. *ACS Energy Lett.* **2020**, *5* (5), 1465−1473.
(43) Brennan, M. C.; Veghte, D. P.; Ford, B. R.; McCleese, C. L.; Loftus, L. M.; McComb, D. W.; Song, Z.; Heben, M. J.; Grusenmeyer, T. A. Photolysis of Mixed Halide Perovskite Nanocrystals. *ACS Energy Lett.* **2023**, *8* (5), 2150−2158.
(44) Merdasa, A.; Bag, M.; Tian, Y.; Källman, E.; Dobrovolsky, A.; Scheblykin, I. G. Super-Resolution Luminescence Microspectroscopy Reveals the Mechanism of Photoinduced Degradation in $CH_3NH_3PbI_3$ Perovskite Nanocrystals. *J. Phys. Chem. C* **2016**, *120* (19), 10711−10719.
(45) Steirer, K. X.; Schulz, P.; Teeter, G.; Stevanovic, V.; Yang, M.; Zhu, K.; Berry, J. J. Defect Tolerance in Methylammonium Lead Triiodide Perovskite. *ACS Energy Lett.* **2016**, *1* (2), 360−366.
(46) Elliott, R. J. Intensity of Optical Absorption by Excitons. *Phys. Rev.* **1957**, *108* (6), 1384−1389.
(47) Ruf, F.; Aygüler, M. F.; Giesbrecht, N.; Rendenbach, B.; Magin, A.; Docampo, P.; Kalt, H.; Hetterich, M. Temperature-Dependent Studies of Exciton Binding Energy and Phase-Transition Suppression in $(Cs,Fa,Ma)Pb(I,Br)_3$ Perovskites. *APL Mater.* **2019**, *7* (3), 031113.
(48) Zhong, X.; Ni, X.; Kaplan, A.; Zhao, X.; Ivancevic, M.; Ball, M. L.; Xu, Z.; Li, H.; Rand, B. P.; Loo, Y.-L.; Brédas, J.; Kahn, A. Evolution of the Electronic and Excitonic Properties in 2D Ruddlesden−Popper Perovskites Induced by Bifunctional Ligands. *Adv. Energy Mater.* **2024**, *14* (18), 2304345.
(49) Zhang, F.; Ullrich, F.; Silver, S.; Kerner, R. A.; Rand, B. P.; Kahn, A. Complexities of Contact Potential Difference Measurements on Metal Halide Perovskite Surfaces. *J. Phys. Chem. Lett.* **2019**, *10* (4), 890−896.
(50) Zhang, F.; Silver, S. H.; Noel, N. K.; Ullrich, F.; Rand, B. P.; Kahn, A. Ultraviolet Photoemission Spectroscopy and Kelvin Probe Measurements on Metal Halide Perovskites: Advantages and Pitfalls. *Adv. Energy Mater.* **2020**, *10* (26), 1903252.
(51) Euvrard, J.; Yan, Y.; Mitzi, D. B. Electrical Doping in Halide Perovskites. *Nat. Rev. Mater.* **2021**, *6* (6), 531−549.
(52) Vigil, J. A.; Wolf, N. R.; Slavney, A. H.; Matheu, R.; Saldivar Valdes, A.; Breidenbach, A.; Lee, Y. S.; Karunadasa, H. I. Halide Perovskites Breathe Too: The Iodide−Iodine Equilibrium and Self-Doping in Cs_2SnI_6. *ACS Cent. Sci.* **2024**, *10* (4), 907−919.
(53) Beal, R. E.; Slotcavage, D. J.; Leijtens, T.; Bowring, A. R.; Belisle, R. A.; Nguyen, W. H.; Burkhard, G. F.; Hoke, E. T.; McGehee, M. D. Cesium Lead Halide Perovskites with Improved Stability for Tandem Solar Cells. *J. Phys. Chem. Lett.* **2016**, *7* (5), 746−751.

(54) Kaplan, A. B.; Burlingame, Q. C.; Holley, R.; Loo, Y.-L. Prospects for Inorganic $CsPbI_3$ Perovskite Solar Cells with Commercially Viable Lifetimes. *Appl. Energy* **2023**, *1* (1), 010901.
(55) Juarez-Perez, E. J.; Ono, L. K.; Maeda, M.; Jiang, Y.; Hawash, Z.; Qi, Y. Photodecomposition and Thermal Decomposition in Methylammonium Halide Lead Perovskites and Inferred Design Principles to Increase Photovoltaic Device Stability. *J. Mater. Chem. A* **2018**, *6* (20), 9604−9612.

https://doi.org/10.1021/jacs.4c08939
J. Am. Chem. Soc. 2024, 146, 33368−33377